NANO LETTERS

2007
Vol. 7, No. 9
2859−2864

GaAs/AlGaAs Nanowire Heterostructures Studied by Scanning Tunneling Microscopy

Lassana Ouattara,[†] Anders Mikkelsen,*[,†] Niklas Sköld,[‡] Jessica Eriksson,[†] Thijs Knaapen,[§] Elizabeta Ćavar,[†] Werner Seifert,[‡] Lars Samuelson,[‡] and Edvin Lundgren[†]

Synchrotron Radiation Research, Lund University, Box 118, 22100 Lund, Sweden, Solid State Physics, Lund University, Box 118, 22100 Lund, Sweden, Technical University Eindhoven, The Netherlands

Received June 29, 2007

ABSTRACT

We directly image the interior of GaAs/AlGaAs axial and radial nanowire heterostructures with atomic-scale resolution using scanning tunneling microscopy. We show that formation of monolayer sharp and smooth axial interfaces are possible even by vapor-phase epitaxy. However, we also find that instability of the ternary alloys formed in the Au seed fundamentally limits axial heterostructure control, inducing large segment asymmetries. We study radial core–shell nanowires, imaging even ultrathin submonolayer shells. We demonstrate how large twinning-induced morphological defects at the wire surfaces can be removed, ensuring the formation of wires with atomically flat sides.

Free-standing semiconductor nanowires, with tailored electronic and optical properties, are very promising as components for devices in physics, chemistry, and biology.[1−8] One of their most important merits is the possibility to grow a huge variety of high precision nanowire heterostructures in a reproducible way.[1−8] The GaAs/AlGaAs materials system with its considerable band gap difference and small lattice mismatch has (for decades) been of particular interest. Planar quantum wells and quantum wire structures has been formed in the GaAs/AlGaAs systems even with the rapid growth method of metal organic vapor-phase epitaxy (MOVPE)[9−10] These systems form the basis for quantum cascade lasers, THz devices, and high-speed electronics.[11−13] Until now, investigations of AlGaAs/GaAs nanowires were mostly focused on core−shell type of heterostructure growth, for which the good lattice matching is of some significance.[14−16] AlGaAs, a wider band gap material, is used to cap the nanowire for passivation, protection against surface related defects, and as an additional means of altering the energy structure within the nanowire. Furthermore, by selectively etching out the GaAs core, this type of structure can be used to form well-defined AlGaAs tubes.[16] Finally, it is fundamentally an interesting materials system for investigating nanowire growth because it is almost completely lattice-matched, leaving out any considerations of strain effects, and in addition, it is extremely well studied for planar growth.[10] The limits of the interface perfection of nanowire heterostructures is still unknown, with some groups reporting 30 nm broad and diffuse interfaces,[3] while others report 1−3 nm sharp interfaces.[4] In fact, it has been proposed that generally sharp interfaces will be difficult to obtain for rapidly growing nanowires. Further, the regularity of the side facets of the nanowires have recently been seriously questioned, as it has been shown that the very common twinning phenomena in nanowires can lead to the formation of large morphological defects on the side facets of the wires,[17] defects which are incidentally only noticed by the correct tilting of the TEM images.[17] To resolve these issues and define the limits on nanowire segment perfection down to the atomic scale, experimental methods are required that directly probe the atomic scale structure and morphology of the wires. One such method is scanning tunneling microscopy (STM), which has shown very impressive results for quantum wells and quantum dots, giving complementary and high-contrast information compared to other imaging methods.[18] We have recently devised a novel crystalline embedding scheme that allows us to directly image the interior of III−V nanowires by STM.[19] We embed the III−V nanowires in a lattice-matched ternary III−V alloy, enabling the cleavage of the wire sample to expose an extremely flat surface for STM measurements. This method, often termed XSTM, makes it possible to study the interior of nanowires (and other III−V nanostructures) with atomic scale resolution.[19−20]

* Corresponding author. E-mail: anders.mikkelsen@sljus.lu.se.
† Synchrotron Radiation Research, Lund University.
‡ Solid State Physics, Lund University.
§ Technical University Eindhoven.

10.1021/nl071550z CCC: $37.00
Published on Web 08/28/2007

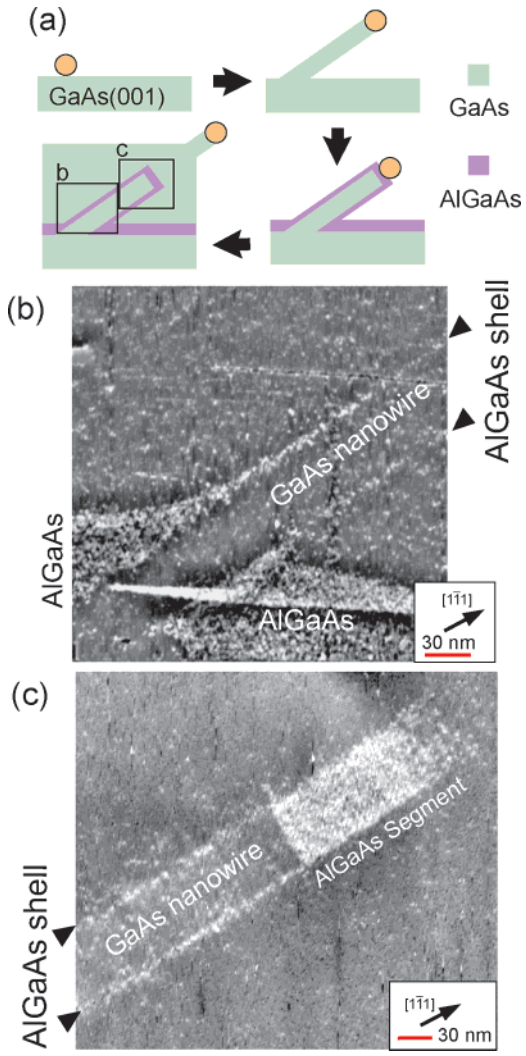

Figure 1. (a) Schematic model of the growth of nanowire heterostructures, which proceeds in three steps after the initial Au nanopartice deposition: GaAs nanowire growth, AlGaAs segment and shell formation, GaAs overgrowth. The wire grow in the [1−11] and [111] directions with 35.3° angles to the substrate. In the model, only the [1−11] direction is shown corresponding to the wire imaged in (b) and (c): (b) 400 × 400 nm^2 STM image of the base of the nanowire; (c) 400 × 400 nm^2 STM image of the AlGaAs segment inside the nanowire

The samples were grown by MOVPE on a Si-doped (001) GaAs substrate, using size-selected Au aerosol particles as seeds. A H_2 carrier gas flow of 6 L/min at a pressure of 100 mbar was used, and a constant flow of arsine was supplied to the reactor cell during the entire process. Prior to growth, the samples were annealed at 580 °C for 10 min. Following the scheme described in Figure 1a, the growth then proceeded in three steps. First, trimethylgallium (TMG) was introduced and regular free-standing 60 nm diameter GaAs nanowires were grown at 450 °C. Second, TMG flow was turned off and the temperature was ramped up to 630 °C in order to overcome the kinetic barrier for side facet growth, and the trimethylaluminum (TMAl) and TMG were introduced simultaneously. Successively, the growth of both an AlGaAs segment at the end of the wire as well as an AlGaAs shell surrounding the wire continued. Simultaneously, an AlGaAs epitaxial layer grew on the substrate. The growth of GaAs was then resumed at the same temperature as the AlGaAs by switching off the TMAl flow. This results in GaAs growth on the wire, shell, and substrate until the lower part of the wire including the AlGaAs structure is completely embedded. Two different sets of samples were grown with different AlGaAs growth times, thus the TMAl was turned on in 20 s and 100 s, respectively, for the two sets of samples. After growth, the samples were transferred to our ultrahigh vacuum (UHV) STM system and cleaved to expose the interior of the nanowires. Images were recorded using commercial Omicron STM1 and XA STM microscopes operated at room temperature. The STMs are positioned inside ultrahigh vacuum systems with base pressures $<1 \times 10^{-10}$ mbar. STM tips used in these experiments were all electrochemically etched tungsten tips, additionally cleaned by Ar sputtering. All images shown were recorded in constant current mode at voltages around −2 to −3 V (filled state imaging) and a feedback current of 0.1−0.2 nA.

As both the core of the nanowire and the embedding material is GaAs, the strong contrast of the AlGaAs in STM[18] is used to clearly identify the wires. In the STM image in Figure 1b, one can see a GaAs nanowire surrounded by an AlGaAs shell extending out from the AlGaAs film along the substrate. The wire makes an angle of 35.3° with the substrate, consistent with one of the usual, [1−11] [−111] growth directions for this type of nanowire on GaAs(001).[19] In Figure 1c, we show a STM image of the AlGaAs segment belonging to the wire in Figure 1b. The segment is found at a distance of 800 nm away from the substrate as measured along the wire. The segment is 130 nm long, but in the top 50 nm, a gradual decrease of the Al content is observed, thus the length of the homogeneous part of the segment is 80 nm.

The high-resolution STM topography of an AlGaAs segment shown in Figure 2 reveals the rows of As atoms inside the wire. First, it can be seen that the As rows visible in Figure 2a, spread in two different directions in well-defined areas. The boundaries of these regions are parallel to the wire growth plane. The two different directions of the As row directions indicate areas of the two different twin crystallites that will generally be found inside III−V nanowires grown in the {111} directions.[17,19] The onset of the AlGaAs can be clearly identified, as the introduction of Al leads to a strong corrugation along the As rows of the AlGaAs as compared to the smooth As rows of the GaAs.[18] It can be observed from Figure 2b that the lower boundary between the GaAs and the AlGaAs segment is monolayer (ML) sharp and smooth. The XSTM results here present a direct way of identifying such sharp interfaces. In the vapor−liquid−solid or vapor−solid−solid models, which are often applied to nanowire growth,[21,22] the 1D growth is based on a supersaturation of wire material in the seed Au particle, leading to an excess of growth material at the interface between the Au particle and the wire. Because the growth rate of the wire is 2−5 monolayers per second, this implies that the Al saturation of the Au particle occurs in less than a second, which is in fact consistent with the high diffusion

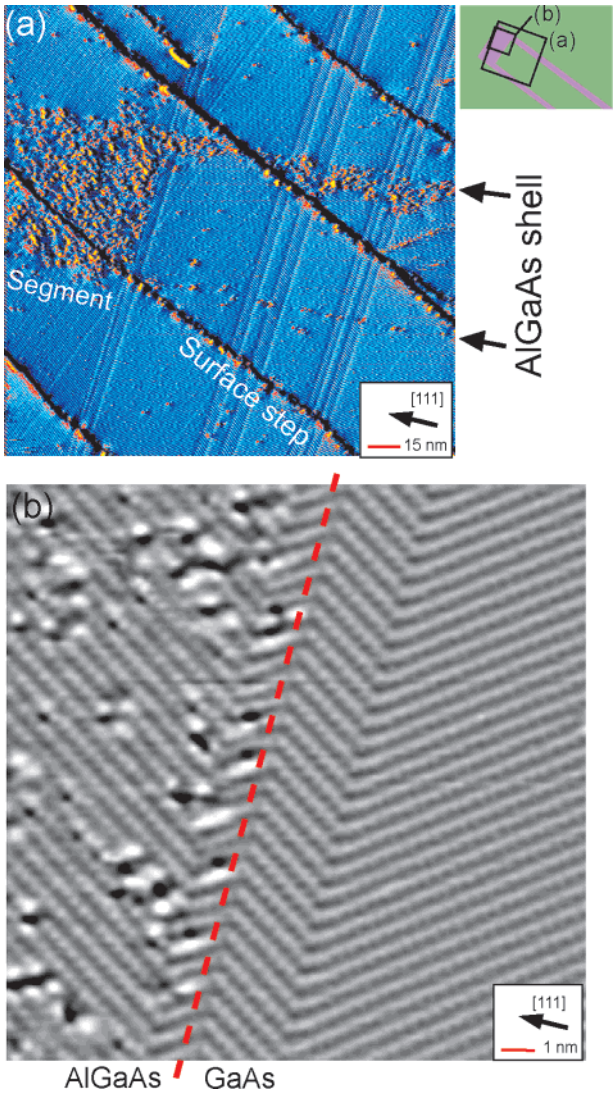

Figure 2. (a) 200 × 200 nm^2 STM image of a nanowire AlGaAs segment and shell. Lines perpendicular to the [1−11] wire growth direction are due to the two types of twin domains. Surface steps due to the cleavage are found with a ∼45° angle in the image. (b) High-resolution 18 × 18 nm^2 STM image of the lower interface between the AlGaAs in the segment and the GaAs in the wire. The atoms seen in the image are As atoms. Thus the strong corrugation in the AlGaAs region is due to the influence on the electronic structure in the As rows due to the Al. The different directions of the As rows indicates areas of the two different types of crystal twins found in this system.

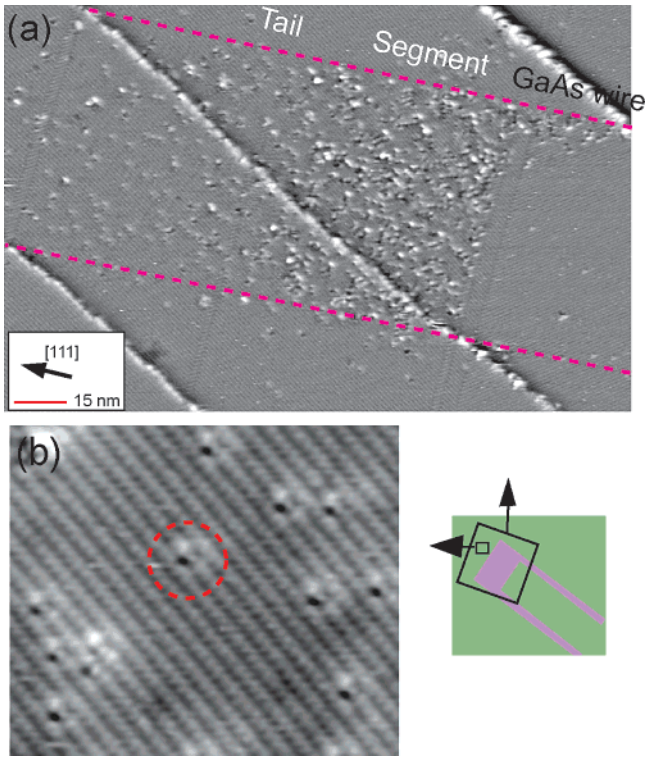

Figure 3. (a) AlGaAs segment and upper diffuse boundary of a nanowire. It can be seen that that the upper boundary extends over 50 nm. (b) Zoom in on Al-related defects in the diffuse tail at the upper boundary. A defect indicative of Al in the first Ga layer is marked by a red circle. This type of defect has been counted to give the Al concentration profile in Figure 4.

rates of Al even in solid Au.[23] We can therefore conclude that the formation of the sharp first interface is due to the instantaneous (<1 s) Al saturation of the Au particle and the subsequent constant release of Al into the wire resulting in the homogeneous AlGaAs segment. The constant Al release continues as long as the Au particle is Al saturated, i.e., as long as Al is supplied from the gas phase. The extremely sharp and smooth interface is also an indication of a layer-by-layer growth mode in the wire. This would indicate a high mobility of the III−V species at the Au−III−V interface and considerable mass transport along this interface. Because As is practically insoluble in the Au particle (at these temperatures), the transport of As to the growth interface must occur through the interface between the Au and the III−V surface.

While the first interface of the AlGaAs segment is sharp, the second boundary is very diffuse with a gradual decrease of the Al content over 50 nm, or ∼150 GaAs monolayers, as seen in Figure 3. In addition, we find that increasing the AlGaAs deposition time a factor of 5 leads to no change in the length of the 50 nm diffuse tail, while the homogeneous part of the AlGaAs segment, the AlGaAs shell, and the AlGaAs substrate film all increases in thickness. The AlGaAs film growing epitaxially on the substrate simultaneously with the wire segment has atomically sharp interfaces at both the top and bottom. If the 50 nm diffuse tail in the wire was a result of residuals in the MOVPE system, an asymmetry should also be found in the AlGaAs at the substrate despite its slower growth rate (asymmetries in AlGaAs films down to the monolayer level have previously been detected with XSTM[18]). Therefore, the slowly decreasing Al content in the top of the wire segment is not related to residual Al material in the MOVPE system. Residual material from the wire sides or the substrate can also be excluded, as this should also lead to a graded upper interface of the AlGaAs at the base of the wire, which has also not been observed in our measurements. Instead, the diffuse boundary must be related to the Al stored in the Au particle. Studying the diffuse part of the AlGaAs segment on the atomic scale as

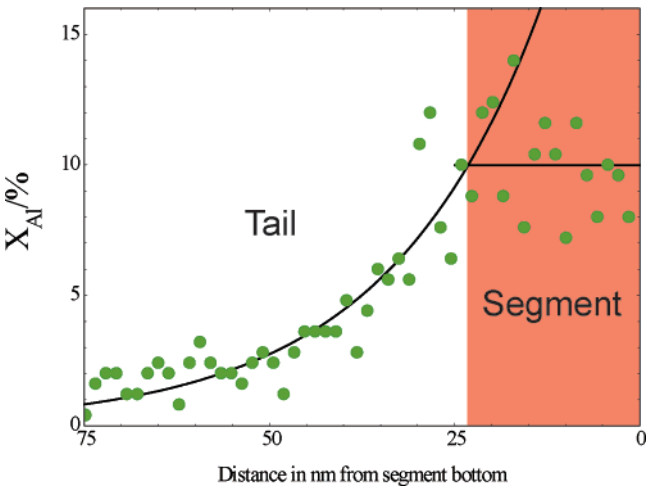

Figure 4. Graph showing the Al concentration profile in the axial AlGaAs segment in a nanowire. The concentration profile was created by counting the Al atoms in the first layers which can be identified as the feature seen in the red circle in Figure 3b.

in Figure 3c, we notice a particular recurring defect (marked by a red circle). This defect is only found in the AlGaAs and is most easily identified in the tail when the Al density is low. The defect geometry has its center in the sites of the top Ga layer, indicating that it is related to changes in this Ga lattice. Considering various possible defects in the Ga lattice and comparing to previous XSTM work on bulk structures,[18] we conclude that this defect is related to Al in the first Ga layer. By counting the defects indicative of Al in the first layer, the Al concentration in each GaAs layer of the wire can then be quantified, as shown on the graph in Figure 4. The nonlinear decrease in Al concentration is consistent with a model in which the Al from the Au particle is gradually incorporated into the nanowire as it continues to grow with the TMAl source off. A crude model can now be developed to fit the segment tail: without a continuous supply of Al to the Au particle from the TMAl, the Al concentration in the particle is diminished as the Al is used for new AlGaAs layers in the nanowire. As discussed above, the diffusion of Al in the Au is so rapid that the Al concentration inside the Au particle has time to equilibrate in between the growth of each layer. As a result, the diminishing concentration of Al in the Au particle will be directly expressed in a diminishing Al concentration in subsequently grown layers in the wire. Assuming this relationship to be linear, one can derive the expression of $C_{Al}(L + 1) = C_{Al}(L)(1 - b)$ for the concentration of Al in the Lth layer of the wire ($L = 0$ is the last monolayer grown before the source of TMAl is turned off). b is the ratio between the amount of group III material in the Au particle and the amount of group III material being incorporated in one layer at nanowire growth front (wire/Au interface). Further we note that the Al and Ga concentrations in ternary AlAuGa alloys can be varied linearly for both high and low Al and Ga concentrations[24] and we assume that b is independent of the Al concentration in the Au particle. By finally setting the concentration of Al in the homogeneous segment to a, $C_{Al}(0) = a$ and the expression $C_{Al}(L) = a(1 - b)^L$ can be derived for the Al concentration in the Lth monolayer of the AlGaAs segment tail. By fitting the model expression, as seen in the graph in Figure 4, we find that $a = 0.096$ and $b = 0.05$. Parameter a indicates that the concentration of Al in the wire segment is ~10% (which can be confirmed by direct estimates of the Al in the segment from the images). In addition, as the number of group III atoms in one nanowire layer is known, parameter b can give the total number of group III atoms in the Au particle, which results in a group III concentration in the particle of 10−20%. This is in reasonable accord with the ~10% Ga content found previously in the Au particle for GaAs wire growth.[25] Further, the amount of Al incorporated into the wire after the TMAl source is turned off can be estimated by integrating the tail of the curve in Figure 4 and multiplying with the number of group III atoms in this section of the wire. This amount of Al corresponds to an Al concentration in the Au seed particle of roughly 1−2%.

Having understood the origin of the nonsharp interface, it is possible to devise general strategies on when and how it can be avoided. First, it is important to note that the problem will only occur when the switching materials are incorporated into the Au particle. The solubility of group V materials in Au is generally negligible, and therefore no group V material reservoir can build up in the particle and all heterostructure interfaces can be sharp. Indeed, there is strong evidence that no such diffuse boundary exists in the case of InP segments in InAs nanowires and GaP segments in GaAs, where the group V material is switched.[4,26] However as escape of group III material from the Au particle seems to happen mostly through growth of the nanowire, our results show that some degree of asymmetry in the heterostructure segments could inherently be hard to avoid for systems where the ternary alloys in the Au particle are not stable.

Turning to the AlGaAs shell, it can be seen in the STM image in Figure 1b that the shell is much thinner than the AlGaAs layers on the substrate and the AlGaAs segment in the wire. The nanowire shell is generally found to be 10 times thinner than the AlGaAs film at the (001) substrate and 30 times thinner than the AlGaAs segment inside the wire. Changing the amount of AlGaAs results in the same relationship between the thicknesses of the AlGaAs shell, segment, and substrate film. Interestingly, by using similar growth parameters, but switching substrate to the GaAs-(111)B, the AlGaAs shell is found to be 20 times thicker. This dramatic difference could be explained by the greater affinity for growth on the GaAs(001) substrates compared to GaAs(111)B substrates. While epitaxial growth is kinetically hindered on the GaAs(111)B, it is more easily achieved on GaAs(001). For chemical beam epitaxy (CBE) growth, it has previously been shown that, for III−V nanowires, up to 80% of the material is supplied from the substrate.[16] While the abundance of materials is larger for MOVPE growth, it is still conceivable that the rapid AlGaAs growth on the (001) substrate will lead to a reduced supply of material for growth of the wire shell, compared to growth on a (111)B substrate.

The detailed atomic scale structure of the AlGaAs shell is shown in Figure 5, and it can again be observed that the

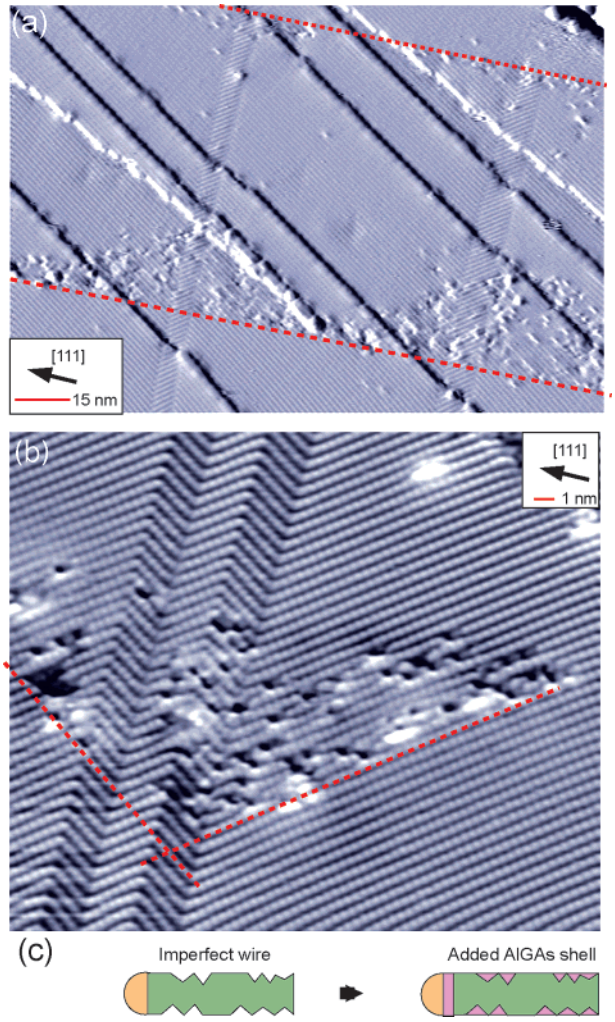

Figure 5. (a) STM image, 200 × 200 nm^2, of the AlGaAs shell; several AlGaAs filled pockets can be seen. The deepest point of the pocket coincides with the twin boundaries. (b) STM images, 30 × 26 nm^2, of high-resolution imaging an AlGAs filled side pocket in the wire. (c) Model of the AlGaAs shell formation as observed in the STM images. The AlGaAs will fill up the pockets in the wires formed at twin boundaries.

As rows, seen in Figure 5c,d (and also Figure 2b,c), run in two different directions identifying the two distinct twin regions. The structure of the twin segments extends beyond the wire into the embedding AlGaAs and GaAs, with the embedding materials adopting the exact crystal structure of the nanowire.

In areas with many alternating twin segments, the thickness of the AlGaAs shell is observed to be far from homogeneous. While long stretches of a submonolayer thin shell exists, a number of large side pockets of AlGaAs extending into the wire can be observed in Figure 5b. It can also be observed that the deepest point of these pockets (into the wire) coincides with the boundary separating the two different types of twins. Further, the slope of the sides of the pockets are seen to be along the As rows in the two twins. To explain this observation, it can be noted that similar types of imperfections on the sides of the nanowire have also been detected in TEM.[17] This type of faceting was found to be a consequence of the switching from one nanowire twin to another. As twinning is very difficult to avoid in nanowire growth, the side pockets will also be hard to avoid.[17]

Interestingly, it is observed that the AlGaAs in the side pockets do not extend beyond the original dimensions of the nanowire. When they are filled up and aligned with the "normal" AlGaAs shell, the rapid growth in the pockets comes to a halt. Previous studies of GaAs/AlGaAs pyramid growth from a masked GaAs(111)B surfaces[27] can be used to understand these results. The AlGaAs was found to grow from triangular openings in a SiO_2 mask as a truncated pyramid with {110} side planes and a (111)B top facet. As the pyramid grows, the (111)B facet becomes smaller and eventually disappears. Similarly, each side facet in the pockets can act as the openings did in the (111)B surface did, allowing for growth of pyramids with {110} side planes. Incidentally, the previous TEM studies indicated that the pocket facets would be {111}, which is consistent with the directions found in this study. The pyramids will eventually grow together to fill the pockets, forming smooth (110) sides. This is an important observation, as it means that the morphological defects due to twin formation on a GaAs nanowire can be removed by adding an AlGaAs shell. Our measurements demonstrate that such a core−shell structure has an extremely smooth surface where all the significant sidewall defects of the original GaAs wire has been removed to within 1 ML. Generally, nanowires with perfectly smooth sides could be important ingredients in a number of applications, for example, the emerging field of nanowire sensors, where single-molecule recognition will set high demands on the wire surface homogeneity. In the case of pyramid growth out of holes on the (111)B surface, it was further observed that AlGaAs could be exchanged with GaAs to continue the pyramid growth,[27] indicating that GaAs could presumably also be used to fill the pockets.

In the present study, AlGaAs/GaAs nanowire heterostructures with both AlGaAs segments and AlGaAs shells have been directly imaged with atomic-scale resolution by STM. We have shown that the first interface between the GaAs and AlGaAs segments is monolayer sharp, while the second interface between the upper part of the AlGaAs segment and GaAs wire at the top is found to be diffuse, showing a gradual decline in Al concentration over 50 nm. The diffuse second interface was directly related to the Al interdiffusion from the Au seed particle. Furthermore, we presented a study of AlGaAs shell formation and observed huge differences in growth speed between wire segment, substrate, and wire shell. Interestingly, we can also compare the thickness of the shell for core−shell nanowires grown on different substrates and find more than an order of magnitude higher growth rate of the AlGaAs shell on GaAs(111)B as compared to GaAs(001). Finally, our measurements indicate an approach to remove large morphological defects at the wire surface, tailoring wires with atomically flat side facets even in the presence of twin defects.

Acknowledgment. This work was performed within the Nanometer Structure Consortium at Lund University and was supported by the Swedish Research Council (VR), the Swedish Foundation for Strategic Research (SSF), the

Crafoord Foundation, the Knut and Alice Wallenberg Foundation, and the EC NoE SANDIE (contract no. NMP4-CT-2004500101).

References

(1) Lieber, C. M. *Sci. Am.* **2001**, *285*, 58−64.
(2) Samuelson, L. *Mater. Today* **2003**, *6* (10), 22
(3) Gudiksen, M. S.; Lauhon, L. J.; Wang, D.; Lieber, C. M. *Nature* **2002**, *415*, 617.
(4) Björk, M. T. et al. *Nano Lett.* **2002**, *2*, 87.
(5) Lauhon, L. J.; Gudiksen, M. S.; Wang, D.; Lieber, C. M. *Nature* **2002**, *420*, 57.
(6) Sköld, N.; Karlsson, L. S.; Larsson, M. W.; Pistol, M.-E.; Seifert, W.; Tragardh, J.; Samuelson, L. *Nano Lett.* **2005**, *5*, 1943.
(7) Thelander, C.; Nilsson, H. A.; Jensen, L. E.; Samuelson, L. *Nano Lett.* **2005**, *5*, 635−638.
(8) Cui, Y.; Wei, Q. Q.; Park, H. K.; Lieber, C. M. *Science* **2001**, *293*, 1289.
(9) Gustafsson, A.; Samuelson, L.; Malm, J.-O.; Vermeire, G.; Demeester, P. *Appl. Phys. Lett.* **1994**, *64*, 695.
(10) Stringfellow, G. B. *Organometallic Vapor-Phase Epitaxy*, 2nd ed.; Academic Press: New York, 1999.
(11) Faist, J.; Capasso, F.; Sivco, D. L.; Sirtori, C.; Hutchinson, A. L.; Cho, A.Y. *Science* **1994**, *264*, 553.
(12) Köhler, R.; Tredicucci, A.; Beltram, F.; Beere, H. E.; Linfield, E. H.; Davies, A. G.; Ritchie, D. A.; Iotti, R. C.; Rossi, F. *Nature* **2002**, *417*, 159.
(13) Basco, R.; Agahi, F.; Lau, K. M. *Appl. Phys. Lett.* **1993**, *63*, 1960.
(14) Tateno, K.; Gotoh, H.; Watanabe, Y. *Appl. Phys. Lett.* **2004**, *85*, 1808.
(15) Wu, Z. H.; Sun, M.; Mei, X. Y.; Ruda, H. E. *Appl. Phys. Lett.* **2004**, *85*, 657.
(16) Noborisaka, J.; Motohisa, J.; Hara, S.; Fukui, T. *Appl. Phys. Lett.* **2005**, *87*, 093109.
(17) Johansson, J.; Karlsson, L. S.; Svensson, C. P. T.; Mårtensson, T.; Wacaser, B. A.; Deppert, K.; Samuelson, L.; Seifert, W. *Nat. Mater.* **2006**, *5*, 574.
(18) Yu, E. T. *Chem. Rev.* **1997**, *97*, 1017.
(19) Mikkelsen, A.; Sköld, N.; Quattara, L.; Borgström, M.; Andersen, J. N.; Samuelson, L.; Seifert, W.; Lundgren, E. *Nat. Mater.* **2004**, *3*, 519.
(20) Mikkelsen, A.; Lundgren, E. *Prog. Surf. Sci.* **2005**, *80*, 1.
(21) Wagner, R. S. In *Whisker Technology*; Levitt, A. P., Ed.; Wiley-Interscience: New York, 1970; pp 47−119.
(22) Persson, A. I.; Larsson, M. W.; Stenström, S.; Ohlsson, B. J.; Samuelson, L.; Wallenberg, L. R. *Nat. Mater.* **2004**, *3*, 677.
(23) Hirvonen, J. *J. Appl. Phys.* **1981**, *52*, 6143.
(24) Prince, A.; Raynor, G. V.; Evans, D. S. *Phase Diagrams of Ternary Gold Alloys*; The Institute of Metals: London, 1990.
(25) Dick, K. A. et al. *Adv. Func. Mater.* **2005**, *15*, 1603.
(26) Jensen, L. E. et al. *Nano Lett.* **2004**, *4*, 1961.
(27) Fukui, T.; Saito, H.; Kasu, M.; Ando, S. *J. Cryst. Growth* **1992**, *124*, 493.

NL071550Z